Phase Transformation, Hydrogen Absorption/Desorption and Electrochemical Properties of a Novel AB$_{4.5}$-type La$_{0.8}$Mg$_{0.2}$Ni$_{4.0}$Co$_{0.5}$ Alloy

Jingjing Liu[1], Yujun Chai[2], Ning Wang[3,]*

[1] School of Mechanical Engineering, Yangzhou University, Yangzhou 225127, P. R. China
[2] School of Chemistry and Materials Science, Hebei Normal University, Hebei, Shijiazhuang 050024, China
[3] Analysis and Testing Centre, Hebei Normal University, Hebei, Shijiazhuang 050024, China
[*]E-mail: hebsjzwn@gmail.com

In this work, the phase transformation, hydrogen storage performance and electrochemical properties of a novel AB$_{4.5}$-type La$_{0.8}$Mg$_{0.2}$Ni$_{4.0}$Co$_{0.5}$ alloy before and after annealing are studied. It is shown that the as-cast alloy contains a CaCu$_5$-type phase and Ce$_2$Ni$_7$- and Pr$_5$Co$_{19}$-type superlattice phases. After annealing at 850 °C for 12 h, the CaCu$_5$- and Ce$_2$Ni$_7$-type phase abundances decrease, while that of the Pr$_5$Co$_{19}$-type phase increases through short atomic diffusion. The *P-C-T* curve of the as-cast alloy exhibits one plateau, while that of the annealed alloy shows two plateaus in both the hydriding and dehydriding processes. Electrochemical results show that phase transformation benefits the alloy's discharge capacity owing to the increase in the total amount of the superlattice phases. The cycling stability is also improved after annealing due to fewer microstrains and defects. In particular, these alloys exhibit excellent high rate discharge capacities of 136 and 128 mAh g^{-1} at 3000 mA g^{-1} for the as-cast and annealed alloys, respectively. The higher capacity of the as-cast alloy is due to the increase in the LaNi$_5$ phase, which is found to desorb hydrogen at higher pressures than the superlattice phases. This alloy system is a promising material for the high-power negative electrodes of Ni/MH batteries.

1. INTRODUCTION

Nickel metal hydride (Ni/MH) batteries are regarded as an ideal energy source owing to their advantages of high power output, safety, nontoxicity, lack of a memory effect and low cost [1-4]. However, further improvements are still needed to satisfy the increasing demand from society [1]. In the

development of Ni/MH batteries, novel negative electrode materials play an essential role and have always been a focus [2, 5-7].

Among the various kinds of negative electrode materials for Ni/MH batteries, $LaNi_5$-based hydrogen storage alloys have been extensively studied and commercialized for years [8, 9]. However, this alloy system suffers from a low discharge capacity due to the limitation of its $CaCu_5$-type structure [5, 10]. Recently, a type of La–Mg–Ni-based alloy with A/B ratios of 3.0–4.0 has attracted much attention. This alloy system contains phases with superlattice structures composed of various ratios of $[A_2B_4]$ and $[AB_5]$ subunits stacking along the c-axis [11]. They have a high discharge capacity because they can store hydrogen not only inside the $[A_2B_4]$ and $[AB_5]$ subunits but also between these subunits. However, their high rate dischargeability (*HRD*) needs to be further improved because of their relatively lower ratio of B-site catalytic elements [1, 12]. Considering that AB_5-type alloys have the advantage of higher Ni content benefiting the fast charge/discharge reaction rates and that La–Mg–Ni-based alloys have high capacity, alloys with an A/B ratio between La–Mg–Ni-based ($AB_{3.0}$–$AB_{4.0}$) and $LaNi_5$-type (AB_5) alloys may have a collaborative effect and compensate for the disadvantages of each other. An $AB_{4.5}$-type $La_{0.62}Mg_{0.08}Ce_{0.2}Y_{0.1}Ni_{3.25}Co_{0.75}Mn_{0.2}Al_{0.3}$ alloy has been reported and has great potential for applications in Ni/MH batteries [12]. However, there are few studies on this alloy system with A/B ratios of 4.0–5.0.

Phase transformation has a great impact on the electrochemical properties of hydrogen storage alloys. Wu's group [13] reported that for the A_2B_7-type $La_{0.75}Mg_{0.25}Ni_{3.05}Co_{0.2}Al_{0.1}Mo_{0.15}$ alloy, decreasing the $LaNi_5$ phase from 23.6 wt.% to 3.1 wt.% and increasing the superlattice phase amounts could improve the alloy's discharge capacity from 339 mAh/g to 375 mAh/g. Zhang's group [14] found that when the $(La,Mg)_2Ni_7$ phase abundance in the AB_3-type $La_{0.67}Mg_{0.33}Ni_3$ alloy increased from 0 to 72 wt.%, the maximum discharge capacity first increased from 360 mAh g^{-1} to 385 mAh g^{-1} and then decreased to 379 mAh g^{-1}, and the *HRD* first increased from 36.6% to 47.5% and then decreased to 45%. Therefore, the phase transformation process and its effect on the electrochemical performance of this novel $AB_{4.0–5.0}$-type alloy system would be interesting to study.

Annealing is believed to be an effective way to induce phase transformation in hydrogen storage alloys, and it usually has a positive effect on the electrochemical properties, especially cycling stability [2, 13, 15]. Moreover, the introduction of foreign elements to partially substitute either the La (Ce, Pr, Nd, etc.) or Ni (Al, Mn, Si, Zn, Cr, Fe, Cu, Co, etc.) sites has also been reported to improve the overall charge/discharge behavior of hydrogen storage alloys [16, 17]. Among all the substituting elements, cobalt is indispensable for maintaining a long cycle life for both AB_5-type alloys and La–Mg–Ni-based alloys [18-20].

Based on the discussion above, in this work, a novel $AB_{4.5}$-type $La_{0.8}Mg_{0.2}Ni_{4.0}Co_{0.5}$ alloy was prepared, and its phase transformation process by annealing was studied. Moreover, the effects of phase transformation on the hydrogen storage and electrochemical properties, as well as the affecting mechanism, are revealed.

2. EXPERIMENTAL

2.1 Alloy preparation

The $La_{0.8}Mg_{0.2}Ni_{3.5}Co_{0.3}$ alloy was prepared by induction melting pure La (99.5 wt%), Ni (99.5 wt%) and Co (99.5 wt%) elements and Mg-Ni alloy under argon atmosphere. 15 wt% of extra Mg was added to compensate for Mg loss during the melting process. During preparation, the alloy was turned over 4 times to ensure that it was as homogenous as possible. After cooling, part of the alloy was broken off and annealed at 850 °C for 24 h under argon atmosphere in a tube furnace.

2.2 XRD measurement

2.2.1 XRD measurement of the as-prepared alloys

The crystal structures of the as-cast and annealed alloys were analyzed by X-ray diffraction (XRD). For this measurement, part of each alloy sample was crushed and ground into powders of ~300 mesh size and measured using an X'pert PRO MPD X-ray diffractometer with Cu Kα radiation. The XRD patterns were refined with the Rietveld method [21] using Rietan-2000 software [22].

2.2.2 XRD measurement of the alloys at different hydrogen absorption/desorption stages

To study the phase transformation of the alloys during hydriding/dehydriding, XRD patterns at different hydrogen pressures were measured. First, both the as-cast and annealed alloys after activation were exposed to the designated hydrogen pressure at 70 °C for 30 min to reach equilibrium. Then, the hydride samples were rapidly removed from the chamber and stored in small sealed tubes. Afterwards, XRD measurements were carried out within several minutes. XRD data were collected in the range from 10° to 80°.

2.3 Hydrogen storage properties

The pressure-composition (*P-C*) curves of both the as-cast and annealed alloys were investigated using a Sievert-type apparatus at temperatures in the range of 40~100 °C. Before measurement, these alloys were put placed into stainless steel chambers with a volume of 6 cm^3 and evacuated at 200 °C for at least 2 h under a pressure of 1×10^{-4} Pa to remove impurities. Then, the stainless steel chambers were cooled down to the assigned temperatures. Hydrogen gas with a purity of 99.999% was introduced into the chamber during the hydriding/dehydriding process.

2.4 Electrochemical properties

To prepare the working electrodes, the alloy powders were mixed with carbonyl Ni powder in a weight ratio of 1:5 and cold-pressed into pellets with a diameter of 1 cm. Subsequently, the simulated three-electrode cell system, including a working electrode (metal hydride electrode), a counter electrode

($NiOOH/Ni(OH)_2$) and a reference electrode (Hg/HgO), was installed. Prior to the electrochemical tests, all alloy electrodes were immersed in 6 M KOH aqueous solution for 24 h. To test the activation property, the half cells were charged/discharged at a current density of 60 $mA \cdot g^{-1}$. For cyclic stability measurement, the half cells were charged/discharged at 120 $mA \cdot g^{-1}$ for 80 cycles. The high-rate discharge capacity of these electrodes was measured at varying discharge current densities. The high-rate dischargeability (*HRD*) was calculated according to the following equation:

$$HRD(\%) = (C_n/C_{max}) \times 100\% \qquad (1)$$

where C_{max} denotes the maximum discharge capacity at a current density of 60 $mA \cdot g^{-1}$ and C_n denotes the discharge capacity at the discharge current density of n $mA \cdot g^{-1}$.

3. RESULTS AND DISCUSSION

3.1 Crystal structure

Fig. 1 shows the Rietveld refinement patterns of the as-cast and annealed $La_{0.8}Mg_{0.2}Ni_{4.0}Co_{0.5}$ alloys. They are composed of Ce_2Ni_7-type $(La,Mg)_2(Ni,Co)_7$, Pr_5Co_{19}-type $(La,Mg)_5(Ni,Co)_{19}$ and $CaCu_5$-type $La(Ni,Co)_5$ phases. The first two phases are composed of superlattice structures with $[(La,Mg)_2(Ni,Co)_4]$ and $[La(Ni,Co)_5]$ subunits stacking along the c-axis in ratios of 1:2 and 1:3, respectively. The phase abundances of the as-cast alloy are 21.3 wt%, 25.3 wt% and 53.4 wt% for Ce_2Ni_7-, Pr_5Co_{19}- and $CaCu_5$-type phases, respectively. After annealing at 850 °C for 24 h, the phase abundances are 18.9 wt% (Ce_2Ni_7-type), 38.5 wt% (Pr_5Co_{19}-type) and 42.6 wt% ($CaCu_5$-type). Part of the Ce_2Ni_7- and $CaCu_5$-type phases was converted into the Pr_5Co_{19}-type phase. As the annealing temperature is much lower than the peritectic reaction temperature of the Pr_5Co_{19}-type phase [23], the reaction process is considered short atomic diffusion.
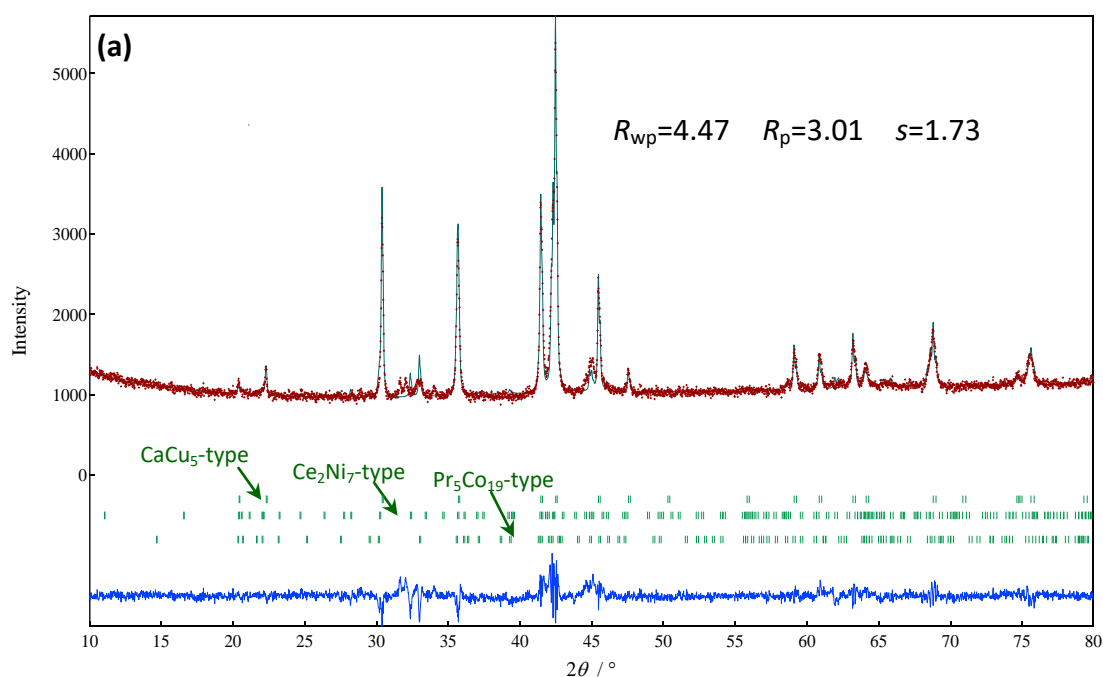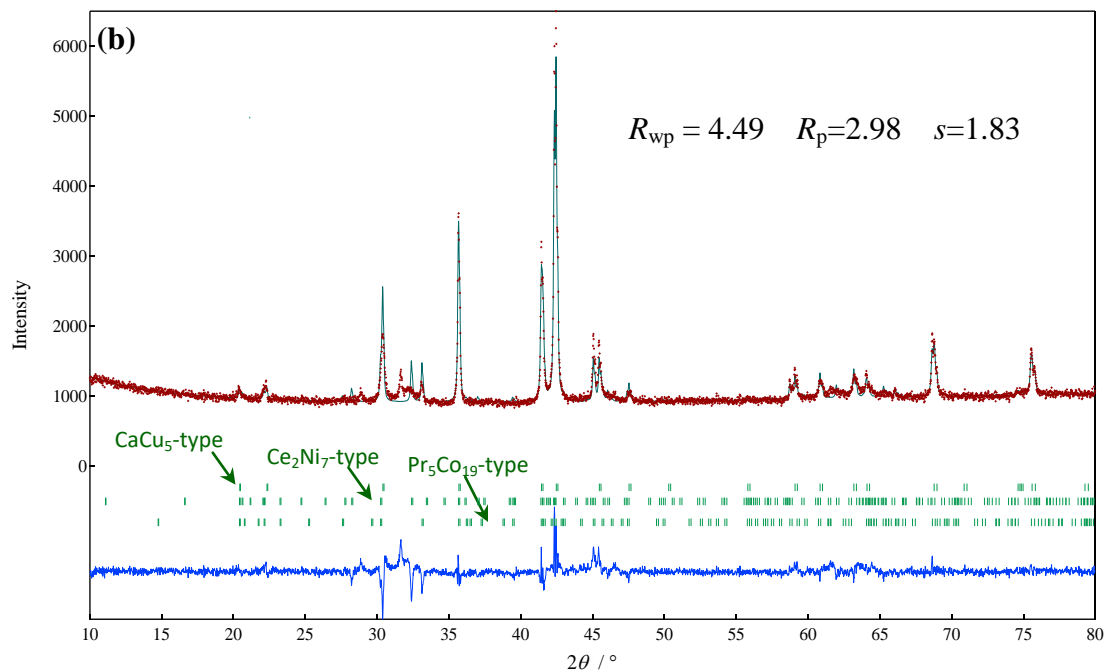
Figure 1. XRD profiles of the as-cast **(a)** and annealed **(b)** $La_{0.8}Mg_{0.2}Ni_{4.0}Co_{0.5}$ alloys. $CaCu_5$-type, Pr_5Co_{19}-type and Ce_2Ni_7-type phases are used as the model. The phase peaks are shown with vertical bars, and the difference between the observed and calculated profiles is shown with the blue line below.

3.2 Hydrogen storage properties

The *P-C* isotherms of the as-cast and annealed alloys at various cycles at 70 °C are shown in Fig. 2. The as-cast alloy exhibits a single plateau during both the hydrogen absorption and desorption processes, while the annealed alloy shows two plateaus. Both the as-cast and annealed alloys are composed of the $CaCu_5$-type phase and the superlattice phases. The equilibrium pressure of the superlattice phases is lower than that of the $CaCu_5$-type phase [24, 25]. Theoretically, the superlattice phases are hydrided first, followed by the $CaCu_5$-type phase [26]. However, only one plateau was observed for the as-cast alloy (Fig. 2 (a)). In contrast, two plateaus were observed for the annealed alloy (Fig. (2b)). These phenomena are similar to our previous results [24]. For the as-cast alloy, the melted metal liquid was quickly solidified by water cooling in the preparation process, which resulted in the disordered distribution of each phase. Therefore, it was conjectured that the *P-C* curves of the as-cast alloy show the simultaneous hydriding of both the superlattice phases and the $CaCu_5$-type phase. In this state, the energy is very high. In contrast, in the annealing process, the high temperature allows the atoms to migrate to an equilibrium position where the atoms are more regularly arranged, benefiting the separation arrangement of the alloy phases. Therefore, two distinguishable hydrogen absorption/desorption processes are observed in the *P-C* curves.
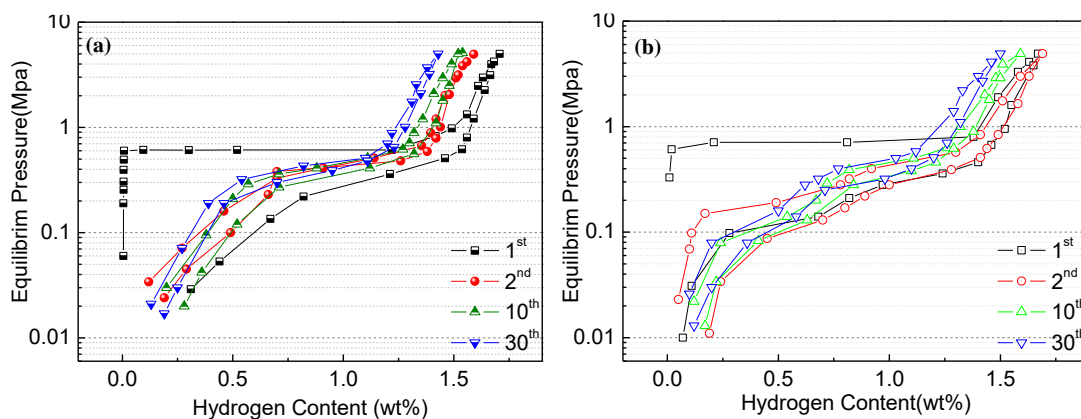
Figure 2. *P-C* curves at different cycles of as-cast **(a)** and annealed **(b)** $La_{0.8}Mg_{0.2}Ni_{4.0}Co_{0.5}$ alloys at 70 °C.

Both the as-cast and annealed $La_{0.8}Mg_{0.2}Ni_{4.0}Co_{0.5}$ alloys exhibit high hydrogen storage capacity at 70 ° C, of 1.68 wt% and 1.71 wt%, respectively, during the first cycle. Two factors influence the hydrogen storage capacity of the alloys. On one hand, the total amount of the superlattice phases increases with the decrease in the $CaCu_5$-type phase abundance, which benefits the hydrogen storage capacity; on the other hand, the Ce_2Ni_7-type phase, which has the highest theoretical capacity among the three phases, decreases, reducing the hydrogen storage capacity. These two combined effects result in the slightly higher capacity of the alloy after annealing. After 30 cycles, the remaining capacities are 83.6% (1.43 wt%) and 89.3% (1.50 wt%) for the as-cast and annealed alloys, respectively. The higher capacity retention of the annealed alloy is due to the decrease in microstrains after heat treatment, which further relives the destruction of the crystal structure.
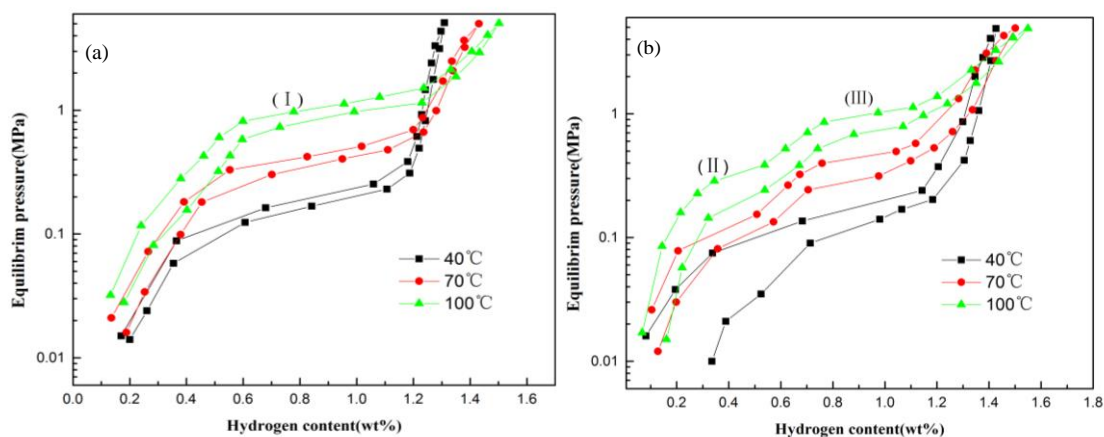

Figure 3. *P-C-T* curves of the as-cast **(a)** and annealed **(b)** $La_{0.8}Mg_{0.2}Ni_{4.0}Co_{0.5}$ alloys at different temperatures.

The *P-C* curves of the as-cast and annealed $La_{0.8}Mg_{0.2}Ni_{4.0}Co_{0.5}$ alloys at different temperatures were consecutively measured after activation under 5 MPa (Fig. 3). The equilibrium pressure increases with increasing temperature from 40 °C to 100 °C. The two plateaus were preserved over a wide temperature range for the annealed alloy (Fig. 3 (b)), and only one was preserved for the as-cast alloy

(Fig. 3 (b)). The hydride formation enthalpies were calculated according to the Van't Hoff equation: $\ln P_{H2} = \triangle H/RT - \triangle S/R$, where R is the ideal gas constant and T is the absolute temperature [27]. The Van't Hoff plots are drawn in Fig. 4. For the annealed alloy, $\triangle H$ values are -23 kJ/mol (II) and -28 kJ/mol (III) for the lower and higher plateau, respectively. The $\triangle H$ for the as-cast alloy is -28 kJ/mol (I). This result indicates that the hydriding transformation process of the as-cast alloy is similar to the higher plateau of the annealed alloy.
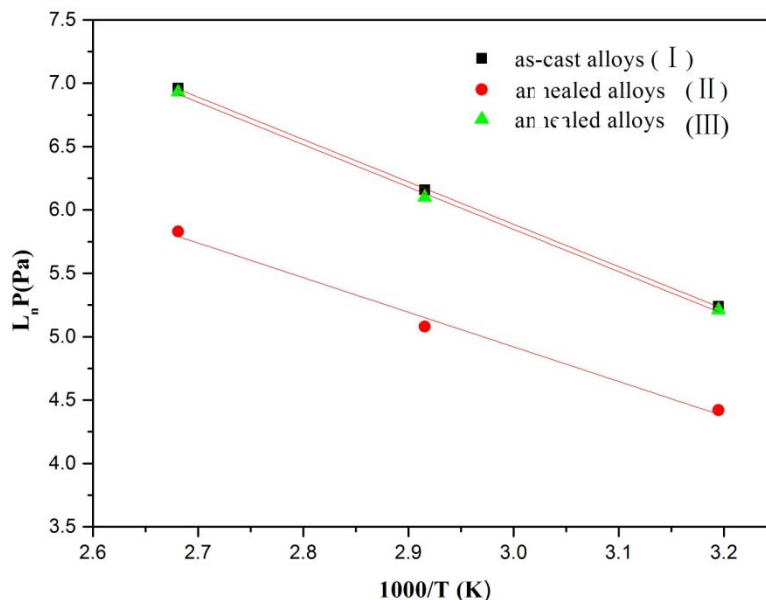
Figure 4. Van't Hoff plots for as-cast and annealed $La_{0.8}Mg_{0.2}Ni_{4.0}Co_{0.5}$ alloys.

3.3 Electrochemical properties

        Fig. 5 shows the discharge curves of the as-cast and annealed $La_{0.8}Mg_{0.2}Ni_{4.0}Co_{0.5}$ alloys. For both alloys, the discharge curves exhibit one flat discharge plateau and a small turning point at ~1.0 V. The small turning point is considered to be related to the multiphase compositions [16]. The discharge capacities of the as-cast and annealed alloys are 349 mAh·g^{-1} and 367 mAh·g^{-1}, respectively, as shown in Fig. 6. Annealing improves the discharge capacity, which is in agreement with the hydrogen storage capacity of *P-C* isotherms. The electrochemical properties of alloys with similar electrode materials for Ni/MH batteries are shown in Table 1. Generally, the discharge capacity of the alloys electrodes decreases with increasing B/A ratio. But the difference is not very significant. It should be noted that the alloys in the table have all went through heat treatment except for the as-cast $La_{0.8}Mg_{0.2}Ni_{4.0}Co_{0.5}$ alloy in the present study, and that's why its capacity is relatively lower. After 80 cycles, the discharge capacities remain 235 mAh·g^{-1} and 255 mAh·g^{-1} for the as-cast and annealed alloys, corresponding to cycling retentions of 67.3% and 69.5%, respectively. The cycling retentions of the alloy electrodes in this study are relatively low compared with most of the alloys in Table 1. This is probably because of the large amount of $LaNi_5$ phase coexisting with superlattice phases. It is reported that $LaNi_5$ phase has

a discrete lattice expansion/contraction with the superlattice phases during hydrogen absorption/desorption [28], accelerating the degradation of the alloys.
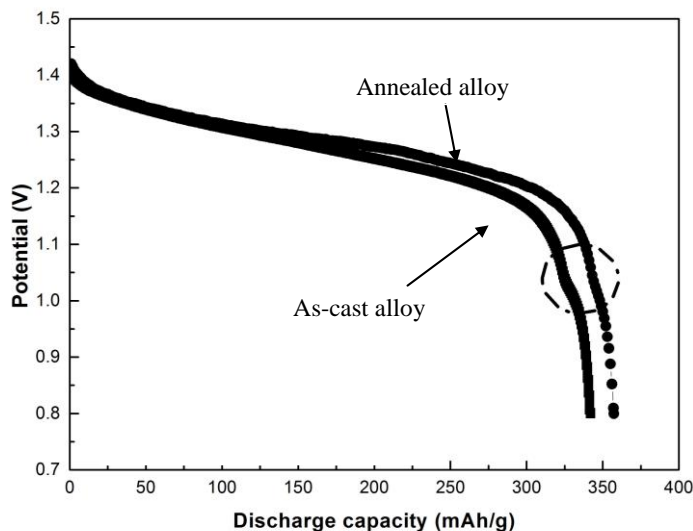

Figure 5. Discharge curves of as-cast and annealed $La_{0.8}Mg_{0.2}Ni_{4.0}Co_{0.5}$ alloys

Table 1. Summary of performances of hydrogen storage alloys for Ni-MH batteries.

|	Capacity performance	Cycling performance	*HRD*	Reference
$La_{0.67}MgNi_3$ (annealed)	398 mAh g^{-1} at 0.25 C	61% after 100 cycles	52.7% at 1200 mA g^{-1}	[29]
$La_{0.75}Mg_{0.25}Ni_{3.2}$ (annealed)	379 mAh g^{-1} at 0.2 C	63% after 100 cycles	64% at 1500 mA g^{-1}	[30]
$La_{0.78}Mg_{0.22}Ni_{3.4}$ (annealed)	377 mAh g^{-1} at 0.2 C	73% after 100 cycles	43.0% at 1500 mA g^{-1}	[30]
$La_{0.75}Mg_{0.25}Ni_{3.5}$ (annealed)	391 mAh g^{-1} at 0.25 C	82% after 150 cycles	92.3% at 900 mA g^{-1}	[31]
$La_{0.81}Mg_{0.19}Ni_{3.6}$ (annealed)	370 mAh g^{-1} at 0.2 C	64% after 100 cycles	43.0% at 1500 mA g^{-1}	[30]
$La_{0.76}Mg_{0.24}Ni_{3.62}$ (annealed)	388 mAh g^{-1} at 0.2 C	85% after 100 cycles	49.7% at 1500 mA g^{-1}	[32]
$La_{0.79}Mg_{0.21}Ni_{3.71}$ (annealed)	374 mAh g^{-1} at 0.2 C	83% after 100 cycles	53.2% at 1500 mA g^{-1}	[32]
$La_{0.8}Mg_{0.2}Ni_{4.0}Co_{0.5}$ (as-cast)	349 mAh g^{-1} at 0.2 C	67.3% after 80 cycles	41.1% at 3000 mA g^{-1}	This work
$La_{0.8}Mg_{0.2}Ni_{4.0}Co_{0.5}$ (annealed)	367 mAh g^{-1} at 0.2 C	69.5% after 80 cycles	36.8% at 3000 mA g^{-1}	This work
$La_{0.62}Mg_{0.08}Ce_{0.2}Y_{0.1}Ni_{3.25}Co_{0.75}$ $Mn_{0.2}Al_{0.3}$ (annealed)	327 mAh g^{-1} at 0.2 C	80% after 928 cycles	32.1% at 3000 mA g^{-1}	[33]
$La_{0.7}Ce_{0.3}Ni_{4.2}Mn_{0.9}Cu_{0.37}$ (annealed)	323 mAh g^{-1} at 0.2 C	79% after 100 cycles	60.1% at 1200 mA g^{-1}	[34]
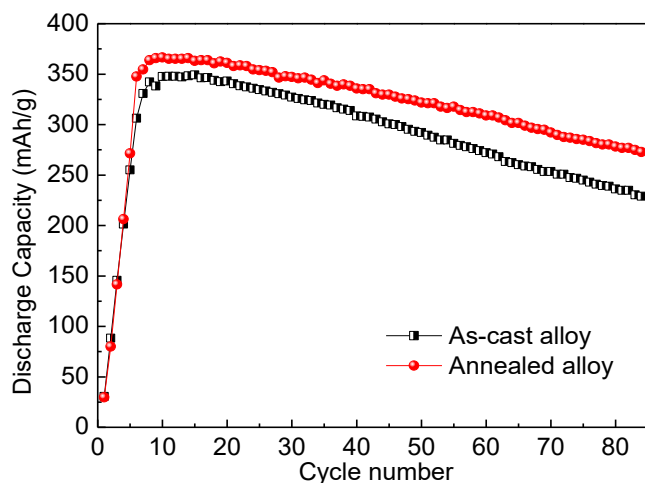
Figure 6. Discharge capacity of as-cast and annealed $La_{0.8}Mg_{0.2}Ni_{4.0}Co_{0.5}$ alloys within 80 cycles.

The effect of annealing on the battery cycling stability is less obvious than that of the gaseous cycling stability. This is because, in addition to the destruction of crystal structures, oxidation/corrosion is also a significant factor causing capacity loss in the battery. The oxidation/corrosion resistance of the $LaNi_5$ phase is greater than that of the superlattice phases. Therefore, the decrease in the $LaNi_5$ phase abundance in exchange for superlattice phases has a negative effect on the cycling stability. Consequently, the comparison of the cycling stability between these two alloys is the combined effect of the improved crystal structure and less oxidation/corrosion resistance of the annealed alloy.

Fig. 7 shows the discharge capacity and high rate dischargeability (*HRD*) of the as-cast and annealed $La_{0.8}Mg_{0.2}Ni_{4.0}Co_{0.5}$ alloys at various discharge current densities. The discharge capacity of the annealed alloy is higher when the discharge current density is relatively low, but when the discharge current density is greater than 1800 mAh g^{-1}, the discharge capacity of the as-cast alloy becomes higher. This result means that the as-cast alloy has a better high-rate discharge capability. The *HRD* values at all discharge current densities are higher for the as-cast alloy than for the annealed alloy. The discharge capacities of the alloys at 3000 mA·g^{-1} are 136 mAh·g^{-1} (as-cast alloy) and 128 mAh·g^{-1} (annealed alloy), corresponding to *HRD* values of 41.1% and 36.8%, respectively. These values are much higher than those of most of the La−Mg−Ni-based and $LaNi_5$-based alloy electrodes [2−8].
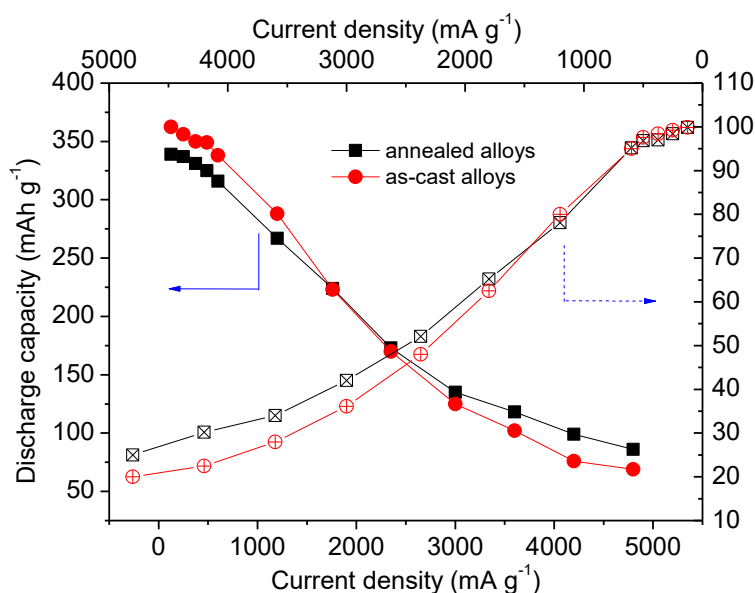

Figure 7. Discharge capacity and high rate dischargeability curves of as-cast and annealed $La_{0.8}Mg_{0.2}Ni_{4.0}Co_{0.5}$ alloys

To analyze the internal reason for the fast discharge capability of the as-cast alloy, Fig. 8 (b)–(c) shows the XRD profiles of the as-cast and annealed $La_{0.8}Mg_{0.2}Ni_{4.0}Co_{0.5}$ alloys at different hydriding/dehydriding stages in the *P-C* isotherms of Fig. 8 (a). Only hydride is observed during hydriding. The peaks shift to lower angles corresponds to the expansion of the lattice parameters. It expands from a=0.5052 nm to 0.5423 nm and c=3.203 nm to 3.498 nm for the Pr_5Co_{19}-type phase and from a=0.5043 nm to 0.5426 nm and c=0.3992 nm to 0.4271 nm for the $CaCu_5$-type phase (Fig. 9).
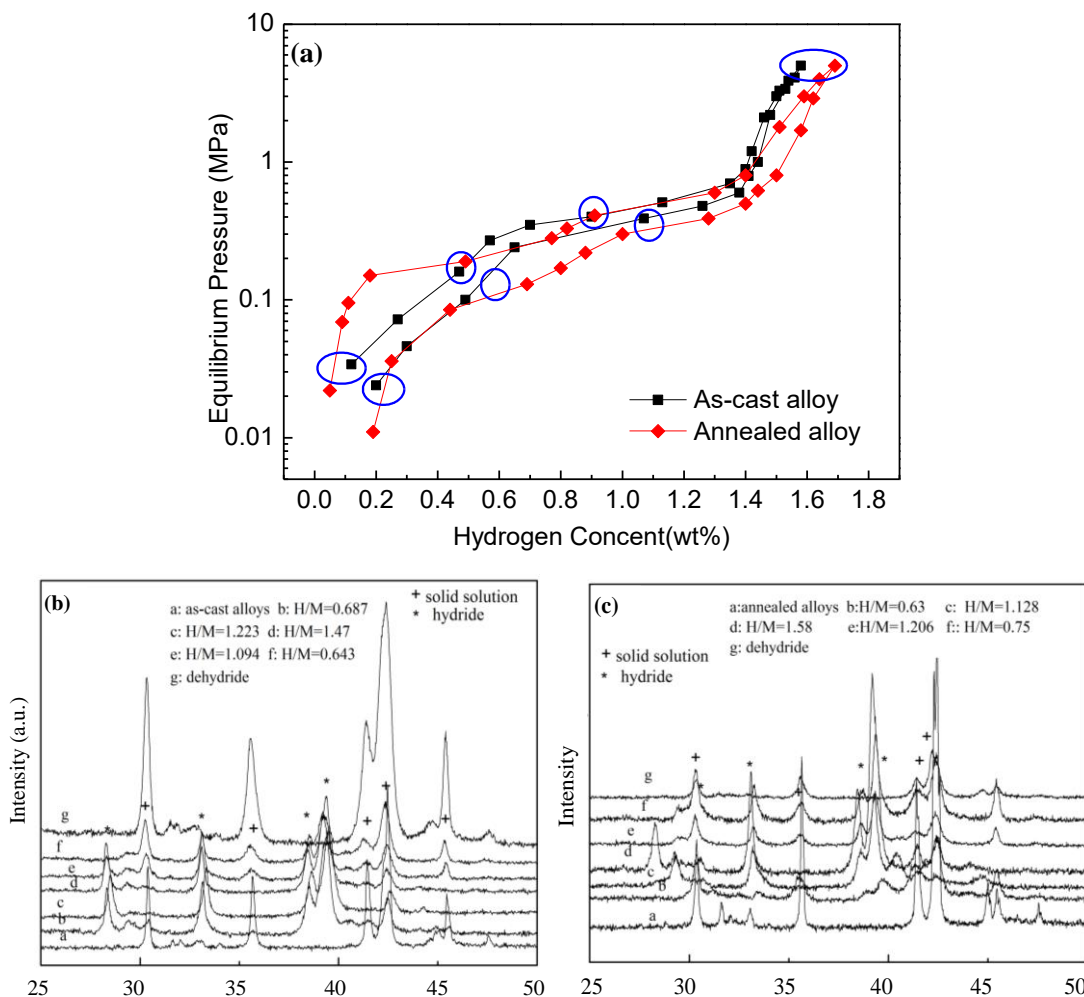
Figure 8. *P-C-T* curves **(a)** and XRD profiles of as-cast **(b)** and annealed **(c)** $La_{0.8}Mg_{0.2}Ni_{4.0}Co_{0.5}$ alloys at different hydriding/dehydriding pressures of (a).

In dehydriding, the peaks shift to higher angles. Moreover, both the solid solution and hydride phases are detected. In view of the XRD results, the hydriding/dehydriding process is described as follows. The hydride phase is observed in hydriding/dehydriding for the Pr_5Co_{19}- and Ce_2Ni_7-type phases [9]. Hence, hydrogen first enters the superlattice phases and forms the hydride phase. In the following hydriding process, the peak splitting is discovered. In contrast, during the dehydriding process, the $CaCu_5$ phase first releases hydrogen. Therefore, the solid solution phase and hydride phase are both detectable. Meanwhile, the XRD profiles of the hydride are suppressed. No obvious difference was observed between the XRD profiles of the as-cast alloy and the annealed alloy, although the phase abundances changed after annealing. This method is not as accurate as in situ XRD, but it is simple to prove that the superlattice phases are first hydrided during hydriding and that the $CaCu_5$-type phase is first hydrided during dehydriding for the $La_{0.8}Mg_{0.2}Ni_{4.0}Co_{0.5}$ alloys. Therefore, the as-cast alloy with a higher $CaCu_5$-type phase abundance shows better high rate dischargeability.
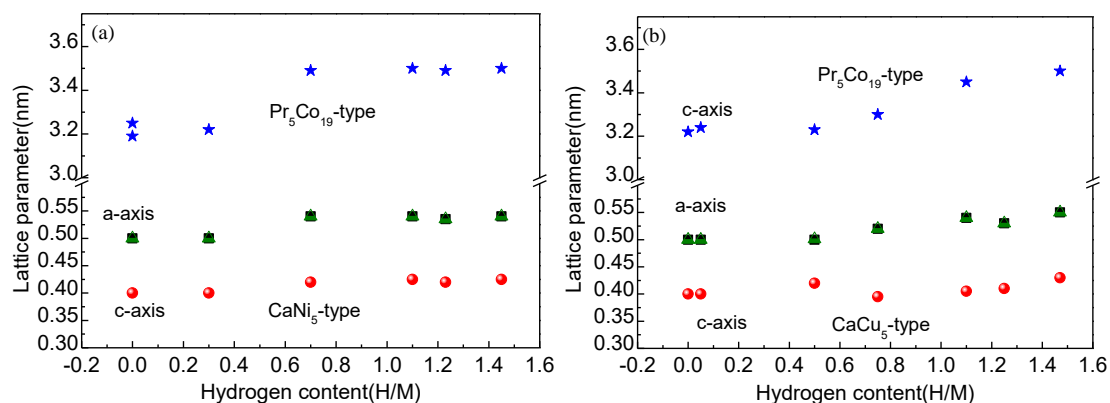
Figure 9. Lattice parameter of $LaNi_5$-type phase and Pr_5Co_{19}-type phase in hydriding/dehydriding **(a)** as-cast alloys **(b)** annealed alloys

4. CONCLUSIONS

The phase transformation, hydrogen storage properties and electrochemical properties of a novel $AB_{4.5}$-type $La_{0.8}Mg_{0.2}Ni_{4.0}Co_{0.5}$ alloy are studied. The main findings are as follows:

a.   The as-cast alloy contains $CaCu_5$-type phase and Pr_5Co_{19}- and Ce_2Ni_7-type superlattice phases. Annealing treatment increases the amount of Pr_5Co_{19}-type phase in sacrifice of $CaCu_5$- and Ce_2Ni_7-type phases during atomic short diffusion process. The total amount of the superlattice phases is increased.

b.   The *P-C* isotherm of the as-cast alloy show single plateau while the annealed one shows double plateaus the higher of which belongs to $CaCu_5$-type phase and the lower one is the combination of Pr_5Co_{19}- and Ce_2Ni_7-type superlattice phases.

c.   Both the gaseous and electrochemical cycling stabilities of the alloys are increased after annealing due to the reduced microstrains in the alloys, which further relives crystal destruction. But as the superlattice phases are more sensitive to electrolyte corrosion and oxidation, the increasing degree is smaller.

d.   Both the as-cast and annealed alloys exhibit good high rate discharge capability. The discharge capacities are 136 and 128 mAh g^{-1} at 3000 mA g^{-1}. The as-cast alloy possesses better *HRD* due to its higher $CaCu_5$-type phase which is proved to be able to desorb hydrogen at higher pressure.

References

1.   L. Zhang, W. Wang, I.A. Rodríguez-Pérez, Y. Zhao, Z.R. Jia, Y. Li, S.M. Han and L.M. Wang, *J.*

Power Sources, 401 (2018) 102.
2. T. Sun, J. Hu, D. Min, T.Z. Luo, Y. Wang, F.M. Xiao, M. Felderhoff, M. Zhu, H. Wang and, R.H. Tang, *Int. J. Hydrogen Energ*y, 43 (2018) 17318.
3. Y. Shi, H.Y. Leng, Q. Luo, S.L. Chen and Q. Li, *Catal. Today*, 2018, In press.
4. Y.F. Liu, H.G. Pan, M.X. Gao and Q.D. Wang, *J. Mater. Chem*., 21 (2011) 474.
5. Y.M. Zhao, S. Zhang, X.X. Liu, W.F. Wang, L. Zhang, Y. Li and S.M. Han, *Int. J. Hydrogen Energ*y, 43 (2018) 17809.
6. L.Z. Ouyang, T.H. Yang, M. Zhu, D. Min, T.Z. Luo, H. Wang, F.M. Xiao and R.H. Tang, *J. Alloys Compd.,* 735 (2018) 98.
7. W. Lv, J.G. Yuan, B. Zhang and Y. Wu, *J. Alloys Compd*., 730 (2018) 360.
8. W.H. Zhou, D. Zhu, Z.Y. Tang, C.L. Wu, L.W. Huang, Z.W. Ma and Y.G. Chen, *J. Power Sources*, 343 (2017) 11.
9. L.Z. Ouyang, J.L. Huang, H. Wang, J.W. Liu and M. Zhu, *Mater. Chem. Phys*., 200 (2017) 164.
10. Y. Li, X.W. Hou, C.X. Wang, L.N. Cheng, X.L. Feng and S.M. Han, *Int. J. Hydrogen Energ*y, 43 (2018) 5104.
11. S. Yasuoka, J. Ishida, K. Kishida and H. Inui, *J. Power Sources*, 346 (2017) 56.
12. C.C. Wang, Y.T. Zhou, C.C. Yang and Q. Jiang, *J. Power Sources*, 398 (2018) 42.
13. W. Li, B. Zhang, J.G. Yuan and Y. Wu, *J. Hydrogen Energ*., 41 (2016) 11767.
14. J.L. Zhang, S.M. Han, Y. Li, J.J. Liu, S.Q. Yang, L. Zhang and J.D. Wang, *J. Alloys Compd*., 581 (2013) 693.
15. X.B. Han, X.J. Yang, P. Wang, W. Chen, Z.F. Lin, G.L. Liu, D.M. Chen and K. Yang, *Rare Metal Mat. Eng.,* 45 (2016) 821.
16. M. Odysseos, P. De Rango, C.N. Christodoulou, E.K. Hlil, T. Steriotis, G. Karagiorgis, G. Charalambopoulou, T. Papapanagiotou, A. Ampoumogli and V. Psycharis, *J. Alloys Compd.,* 580 (2013) S268.
17. Z.X Tan, Y.F. Yang, Y. Li and H.X. Shao, *J. Alloys Compd*., 453 (2008) 79.
18. L. Zhang and S.C. Li, *Rare Metal*s, 34 (2015) 259.
19. I.I. Bulyk, A.M. Trostianchyn, V.G. Synyushko, I.V. Trostianchyn and V.M. Davydov, *Intermetallics*, 13 (2005) 1220–1224.
20. D. Chartouni, K. Gross, *J. Electrochem. Soc.,* 148 (2001) A241.
21. H.M. Rietveld, *J. Appl. Crystallogr*., 2 (1969) 65.
22. Y.J. Chai, K. Sakaki, K. Asano, H. Enoki, E. Akiba and T. Kohno, *Scripta Mater.,* 57 (2007) 545.
23. J.J. Liu, Y. Li, D. Han, S.Q. Yang, X.C. Chen, L. Zhang and S.M. Han, *J. Power Sources*, 300 (2015) 77.
24. J. Gao, X.L. Yan, Z.Y. Zhao, Y.J. Chai and D.L. Hou, J. Power *Sources,* 209 (2012) 257.
25. X.B. Zhang, D.Z. Sun, W.Y. Yin, Y.J. Chai and M.S. Zhao, *Electrochim. Acta*, 50 (2005) 2911.
26. Q.A. Zhang, M. Fang, T.Z. Si, F. Fang, D.L. Sun, L.Z. Ouyang and M. Zhu, *J. Phy. Chem.,* 114 (2010) 11686.
27. K. Young, T. Ouchi, B. Reichman, J. Koch and M.A. Fetcenko, *J. Alloys Compd.,* 509 (2011) 3995.